

Observation of the $\chi_{c2}(2P)$ meson in the reaction $\gamma\gamma \rightarrow D\bar{D}$ at BABAR

B. Aubert,¹ Y. Karyotakis,¹ J. P. Lees,¹ V. Poireau,¹ E. Prencipe,¹ X. Prudent,¹ V. Tisserand,¹ J. Garra Tico,² E. Grauges,² M. Martinelli,^{3a,3b} A. Palano,^{3a,3b} M. Pappagallo,^{3a,3b} G. Eigen,⁴ B. Stugu,⁴ L. Sun,⁴ M. Battaglia,⁵ D. N. Brown,⁵ B. Hooberman,⁵ L. T. Kerth,⁵ Yu. G. Kolomensky,⁵ G. Lynch,⁵ I. L. Osipenkov,⁵ K. Tackmann,⁵ T. Tanabe,⁵ C. M. Hawkes,⁶ N. Soni,⁶ A. T. Watson,⁶ H. Koch,⁷ T. Schroeder,⁷ D. J. Asgeirsson,⁸ C. Hearty,⁸ T. S. Mattison,⁸ J. A. McKenna,⁸ M. Barrett,⁹ A. Khan,⁹ A. Randle-Conde,⁹ V. E. Blinov,¹⁰ A. D. Bukin,^{10,*} A. R. Buzykaev,¹⁰ V. P. Druzhinin,¹⁰ V. B. Golubev,¹⁰ A. P. Onuchin,¹⁰ S. I. Serednyakov,¹⁰ Yu. I. Skovpen,¹⁰ E. P. Solodov,¹⁰ K. Yu. Todyshev,¹⁰ M. Bondioli,¹¹ S. Curry,¹¹ I. Eschrich,¹¹ D. Kirkby,¹¹ A. J. Lankford,¹¹ P. Lund,¹¹ M. Mandelkern,¹¹ E. C. Martin,¹¹ D. P. Stoker,¹¹ H. Atmacan,¹² J. W. Gary,¹² F. Liu,¹² O. Long,¹² G. M. Vitug,¹² Z. Yasin,¹² V. Sharma,¹³ C. Campagnari,¹⁴ T. M. Hong,¹⁴ D. Kovalskyi,¹⁴ M. A. Mazur,¹⁴ J. D. Richman,¹⁴ T. W. Beck,¹⁵ A. M. Eisner,¹⁵ C. A. Heusch,¹⁵ J. Kroseberg,¹⁵ W. S. Lockman,¹⁵ A. J. Martinez,¹⁵ T. Schalk,¹⁵ B. A. Schumm,¹⁵ A. Seiden,¹⁵ L. O. Winstrom,¹⁵ C. H. Cheng,¹⁶ D. A. Doll,¹⁶ B. Echenard,¹⁶ F. Fang,¹⁶ D. G. Hitlin,¹⁶ I. Narsky,¹⁶ P. Ongmongkolkul,¹⁶ T. Piatenko,¹⁶ F. C. Porter,¹⁶ R. Andreassen,¹⁷ M. S. Dubrovin,¹⁷ G. Mancinelli,¹⁷ B. T. Meadows,¹⁷ K. Mishra,¹⁷ M. D. Sokoloff,¹⁷ P. C. Bloom,¹⁸ W. T. Ford,¹⁸ A. Gaz,¹⁸ J. F. Hirschauer,¹⁸ M. Nagel,¹⁸ U. Nauenberg,¹⁸ J. G. Smith,¹⁸ S. R. Wagner,¹⁸ R. Ayad,^{19,†} W. H. Toki,¹⁹ E. Feltresi,²⁰ A. Hauke,²⁰ H. Jasper,²⁰ T. M. Karbach,²⁰ J. Merkel,²⁰ A. Petzold,²⁰ B. Spaan,²⁰ K. Wacker,²⁰ M. J. Kobel,²¹ K. R. Schubert,²¹ R. Schwierz,²¹ D. Bernard,²² E. Latour,²² M. Verderi,²² P. J. Clark,²³ S. Playfer,²³ J. E. Watson,²³ M. Andreotti,^{24a,24b} D. Bettoni,^{24a} C. Bozzi,^{24a} R. Calabrese,^{24a,24b} A. Cecchi,^{24a,24b} G. Cibinetto,^{24a,24b} E. Fioravanti,^{24a,24b} P. Franchini,^{24a,24b} E. Luppi,^{24a,24b} M. Menerato,^{24a,24b} M. Negrini,^{24a,24b} A. Petrella,^{24a,24b} L. Piemontese,^{24a} V. Santoro,^{24a,24b} R. Baldini-Ferrolì,²⁵ A. Calcaterra,²⁵ R. de Sangro,²⁵ G. Finocchiaro,²⁵ S. Pacetti,²⁵ P. Patteri,²⁵ I. M. Peruzzi,^{25,‡} M. Piccolo,²⁵ M. Rama,²⁵ A. Zallo,²⁵ R. Contri,^{26a,26b} E. Guido,^{26a,26b} M. Lo Vetere,^{26a,26b} M. R. Monge,^{26a,26b} S. Passaggio,^{26a} C. Patrignani,^{26a,26b} E. Robutti,^{26a} S. Tosi,^{26a,26b} M. Morii,²⁷ A. Adametz,²⁸ J. Marks,²⁸ S. Schenk,²⁸ U. Uwer,²⁸ F. U. Bernlochner,²⁹ H. M. Lacker,²⁹ T. Lueck,²⁹ A. Volk,²⁹ P. D. Dauncey,³⁰ M. Tibbetts,³⁰ P. K. Behera,³¹ M. J. Charles,³¹ U. Mallik,³¹ C. Chen,³² J. Cochran,³² H. B. Crawley,³² L. Dong,³² V. Eyges,³² W. T. Meyer,³² S. Prell,³² E. I. Rosenberg,³² A. E. Rubin,³² Y. Y. Gao,³³ A. V. Gritsan,³³ Z. J. Guo,³³ N. Arnaud,³⁴ M. Davier,³⁴ D. Derkach,³⁴ J. Firmino da Costa,³⁴ G. Grosdidier,³⁴ F. Le Diberder,³⁴ V. Lepeltier,³⁴ A. M. Lutz,³⁴ B. Malaescu,³⁴ P. Roudeau,³⁴ M. H. Schune,³⁴ J. Serrano,³⁴ V. Sordini,^{34,§} A. Stocchi,³⁴ G. Wormser,³⁴ D. J. Lange,³⁵ D. M. Wright,³⁵ I. Bingham,³⁶ J. P. Burke,³⁶ C. A. Chavez,³⁶ J. R. Fry,³⁶ E. Gabathuler,³⁶ R. Gamet,³⁶ D. E. Hutchcroft,³⁶ D. J. Payne,³⁶ C. Touramanis,³⁶ A. J. Bevan,³⁷ C. K. Clarke,³⁷ F. Di Lodovico,³⁷ R. Sacco,³⁷ M. Sigamani,³⁷ G. Cowan,³⁸ S. Paramesvaran,³⁸ A. C. Wren,³⁸ D. N. Brown,³⁹ C. L. Davis,³⁹ A. G. Denig,⁴⁰ M. Fritsch,⁴⁰ W. Gradl,⁴⁰ A. Hafner,⁴⁰ K. E. Alwyn,⁴¹ D. Bailey,⁴¹ R. J. Barlow,⁴¹ G. Jackson,⁴¹ G. D. Lafferty,⁴¹ T. J. West,⁴¹ J. I. Yi,⁴¹ J. Anderson,⁴² A. Jawahery,⁴² D. A. Roberts,⁴² G. Simi,⁴² J. M. Tuggle,⁴² C. Dallapiccola,⁴³ E. Salvati,⁴³ R. Cowan,⁴⁴ D. Dujmic,⁴⁴ P. H. Fisher,⁴⁴ S. W. Henderson,⁴⁴ G. Sciolla,⁴⁴ M. Spitznagel,⁴⁴ R. K. Yamamoto,⁴⁴ M. Zhao,⁴⁴ P. M. Patel,⁴⁵ S. H. Robertson,⁴⁵ M. Schram,⁴⁵ P. Biassoni,^{46a,46b} A. Lazzaro,^{46a,46b} V. Lombardo,^{46a} F. Palombo,^{46a,46b} S. Stracka,^{46a,46b} L. Cremaldi,⁴⁷ R. Godang,^{47,||} R. Kroeger,⁴⁷ P. Sonnek,⁴⁷ D. J. Summers,⁴⁷ H. W. Zhao,⁴⁷ X. Nguyen,⁴⁸ M. Simard,⁴⁸ P. Taras,⁴⁸ H. Nicholson,⁴⁹ G. De Nardo,^{50a,50b} L. Lista,^{50a} D. Monorchio,^{50a,50b} G. Onorato,^{50a,50b} C. Sciacca,^{50a,50b} G. Raven,⁵¹ H. L. Snoek,⁵¹ C. P. Jessop,⁵² K. J. Knoepfel,⁵² J. M. LoSecco,⁵² W. F. Wang,⁵² L. A. Corwin,⁵³ K. Honscheid,⁵³ H. Kagan,⁵³ R. Kass,⁵³ J. P. Morris,⁵³ A. M. Rahimi,⁵³ S. J. Sekula,⁵³ N. L. Blount,⁵⁴ J. Brau,⁵⁴ R. Frey,⁵⁴ O. Igonkina,⁵⁴ J. A. Kolb,⁵⁴ M. Lu,⁵⁴ R. Rahmat,⁵⁴ N. B. Sinev,⁵⁴ D. Strom,⁵⁴ J. Strube,⁵⁴ E. Torrence,⁵⁴ G. Castelli,^{55a,55b} N. Gagliardi,^{55a,55b} M. Margoni,^{55a,55b} M. Morandin,^{55a} M. Posocco,^{55a} M. Rotondo,^{55a} F. Simonetto,^{55a,55b} R. Stroili,^{55a,55b} C. Voci,^{55a,55b} P. del Amo Sanchez,⁵⁶ E. Ben-Haim,⁵⁶ G. R. Bonneaud,⁵⁶ H. Briand,⁵⁶ J. Chauveau,⁵⁶ O. Hamon,⁵⁶ Ph. Leruste,⁵⁶ G. Marchiori,⁵⁶ J. Ocariz,⁵⁶ A. Perez,⁵⁶ J. Prendki,⁵⁶ S. Sitt,⁵⁶ L. Gladney,⁵⁷ M. Biasini,^{58a,58b} E. Manoni,^{58a,58b} C. Angelini,^{59a,59b} G. Batignani,^{59a,59b} S. Bettarini,^{59a,59b} G. Calderini,^{59a,59b,¶} M. Carpinelli,^{59a,59b,**} A. Cervelli,^{59a,59b} F. Forti,^{59a,59b} M. A. Giorgi,^{59a,59b} A. Lusiani,^{59a,59c} M. Morganti,^{59a,59b} N. Neri,^{59a,59b} E. Paoloni,^{59a,59b} G. Rizzo,^{59a,59b} J. J. Walsh,^{59a} D. Lopes Pegna,⁶⁰ C. Lu,⁶⁰ J. Olsen,⁶⁰ A. J. S. Smith,⁶⁰ A. V. Telnov,⁶⁰ F. Anulli,^{61a} E. Baracchini,^{61a,61b} G. Cavoto,^{61a} R. Faccini,^{61a,61b} F. Ferrarotto,^{61a} F. Ferroni,^{61a,61b} M. Gaspero,^{61a,61b} P. D. Jackson,^{61a} L. Li Gioi,^{61a} M. A. Mazzoni,^{61a} S. Morganti,^{61a} G. Piredda,^{61a} F. Renga,^{61a,61b} C. Voena,^{61a} M. Ebert,⁶² T. Hartmann,⁶² H. Schröder,⁶² R. Waldi,⁶² T. Adye,⁶³ B. Franek,⁶³ E. O. Olaiya,⁶³ F. F. Wilson,⁶³ S. Emery,⁶⁴ L. Esteve,⁶⁴ G. Hamel de Monchenault,⁶⁴ W. Kozanecki,⁶⁴ G. Vasseur,⁶⁴ Ch. Yèche,⁶⁴ M. Zito,⁶⁴ M. T. Allen,⁶⁵ D. Aston,⁶⁵ D. J. Bard,⁶⁵ R. Bartoldus,⁶⁵ J. F. Benitez,⁶⁵ R. Cenci,⁶⁵ J. P. Coleman,⁶⁵ M. R. Convery,⁶⁵ J. C. Dingfelder,⁶⁵ J. Dorfan,⁶⁵ G. P. Dubois-Felsmann,⁶⁵ W. Dunwoodie,⁶⁵ R. C. Field,⁶⁵

M. Franco Sevilla,⁶⁵ B. G. Fulsom,⁶⁵ A. M. Gabareen,⁶⁵ M. T. Graham,⁶⁵ P. Grenier,⁶⁵ C. Hast,⁶⁵ W. R. Innes,⁶⁵ J. Kaminski,⁶⁵ M. H. Kelsey,⁶⁵ H. Kim,⁶⁵ P. Kim,⁶⁵ M. L. Kocian,⁶⁵ D. W. G. S. Leith,⁶⁵ S. Li,⁶⁵ B. Lindquist,⁶⁵ S. Luitz,⁶⁵ V. Luth,⁶⁵ H. L. Lynch,⁶⁵ D. B. MacFarlane,⁶⁵ H. Marsiske,⁶⁵ R. Messner,^{65,*} D. R. Muller,⁶⁵ H. Neal,⁶⁵ S. Nelson,⁶⁵ C. P. O'Grady,⁶⁵ I. Ofte,⁶⁵ M. Perl,⁶⁵ B. N. Ratcliff,⁶⁵ A. Roodman,⁶⁵ A. A. Salnikov,⁶⁵ R. H. Schindler,⁶⁵ J. Schwiening,⁶⁵ A. Snyder,⁶⁵ D. Su,⁶⁵ M. K. Sullivan,⁶⁵ K. Suzuki,⁶⁵ S. K. Swain,⁶⁵ J. M. Thompson,⁶⁵ J. Va'vra,⁶⁵ A. P. Wagner,⁶⁵ M. Weaver,⁶⁵ C. A. West,⁶⁵ W. J. Wisniewski,⁶⁵ M. Wittgen,⁶⁵ D. H. Wright,⁶⁵ H. W. Wulsin,⁶⁵ A. K. Yarritu,⁶⁵ C. C. Young,⁶⁵ V. Ziegler,⁶⁵ X. R. Chen,⁶⁶ H. Liu,⁶⁶ W. Park,⁶⁶ M. V. Purohit,⁶⁶ R. M. White,⁶⁶ J. R. Wilson,⁶⁶ M. Bellis,⁶⁷ P. R. Burchat,⁶⁷ A. J. Edwards,⁶⁷ T. S. Miyashita,⁶⁷ S. Ahmed,⁶⁸ M. S. Alam,⁶⁸ J. A. Ernst,⁶⁸ B. Pan,⁶⁸ M. A. Saeed,⁶⁸ S. B. Zain,⁶⁸ A. Soffer,⁶⁹ S. M. Spanier,⁷⁰ B. J. Wogslund,⁷⁰ R. Eckmann,⁷¹ J. L. Ritchie,⁷¹ A. M. Ruland,⁷¹ C. J. Schilling,⁷¹ R. F. Schwitters,⁷¹ B. C. Wray,⁷¹ B. W. Drummond,⁷² J. M. Izen,⁷² X. C. Lou,⁷² F. Bianchi,^{73a,73b} D. Gamba,^{73a,73b} M. Pelliccioni,^{73a,73b} M. Bomben,^{74a,74b} L. Bosisio,^{74a,74b} C. Cartaro,^{74a,74b} G. Della Ricca,^{74a,74b} L. Lanceri,^{74a,74b} L. Vitale,^{74a,74b} V. Azzolini,⁷⁵ N. Lopez-March,⁷⁵ F. Martinez-Vidal,⁷⁵ D. A. Milanes,⁷⁵ A. Oyanguren,⁷⁵ J. Albert,⁷⁶ Sw. Banerjee,⁷⁶ B. Bhuyan,⁷⁶ H. H. F. Choi,⁷⁶ K. Hamano,⁷⁶ G. J. King,⁷⁶ R. Kowalewski,⁷⁶ M. J. Lewczuk,⁷⁶ I. M. Nugent,⁷⁶ J. M. Roney,⁷⁶ R. J. Sobie,⁷⁶ T. J. Gershon,⁷⁷ P. F. Harrison,⁷⁷ J. Ilic,⁷⁷ T. E. Latham,⁷⁷ G. B. Mohanty,⁷⁷ E. M. T. Puccio,⁷⁷ H. R. Band,⁷⁸ X. Chen,⁷⁸ S. Dasu,⁷⁸ K. T. Flood,⁷⁸ Y. Pan,⁷⁸ R. Prepost,⁷⁸ C. O. Vuosalo,⁷⁸ and S. L. Wu⁷⁸

(BABAR Collaboration)

¹Laboratoire d'Annecy-le-Vieux de Physique des Particules (LAPP), Université de Savoie, CNRS/IN2P3, F-74941 Annecy-Le-Vieux, France

²Universitat de Barcelona, Facultat de Física, Departament ECM, E-08028 Barcelona, Spain

^{3a}INFN Sezione di Bari, I-70126 Bari, Italy

^{3b}Dipartimento di Fisica, Università di Bari, I-70126 Bari, Italy

⁴University of Bergen, Institute of Physics, N-5007 Bergen, Norway

⁵Lawrence Berkeley National Laboratory and University of California, Berkeley, California 94720, USA

⁶University of Birmingham, Birmingham, B15 2TT, United Kingdom

⁷Ruhr Universität Bochum, Institut für Experimentalphysik I, D-44780 Bochum, Germany

⁸University of British Columbia, Vancouver, British Columbia, Canada V6T 1Z1

⁹Brunel University, Uxbridge, Middlesex UB8 3PH, United Kingdom

¹⁰Budker Institute of Nuclear Physics, Novosibirsk 630090, Russia

¹¹University of California at Irvine, Irvine, California 92697, USA

¹²University of California at Riverside, Riverside, California 92521, USA

¹³University of California at San Diego, La Jolla, California 92093, USA

¹⁴University of California at Santa Barbara, Santa Barbara, California 93106, USA

¹⁵University of California at Santa Cruz, Institute for Particle Physics, Santa Cruz, California 95064, USA

¹⁶California Institute of Technology, Pasadena, California 91125, USA

¹⁷University of Cincinnati, Cincinnati, Ohio 45221, USA

¹⁸University of Colorado, Boulder, Colorado 80309, USA

¹⁹Colorado State University, Fort Collins, Colorado 80523, USA

²⁰Technische Universität Dortmund, Fakultät Physik, D-44221 Dortmund, Germany

²¹Technische Universität Dresden, Institut für Kern- und Teilchenphysik, D-01062 Dresden, Germany

²²Laboratoire Leprince-Ringuet, CNRS/IN2P3, Ecole Polytechnique, F-91128 Palaiseau, France

²³University of Edinburgh, Edinburgh EH9 3JZ, United Kingdom

^{24a}INFN Sezione di Ferrara, I-44100 Ferrara, Italy

^{24b}Dipartimento di Fisica, Università di Ferrara, I-44100 Ferrara, Italy

²⁵INFN Laboratori Nazionali di Frascati, I-00044 Frascati, Italy

^{26a}INFN Sezione di Genova, I-16146 Genova, Italy

^{26b}Dipartimento di Fisica, Università di Genova, I-16146 Genova, Italy

²⁷Harvard University, Cambridge, Massachusetts 02138, USA

²⁸Universität Heidelberg, Physikalisches Institut, Philosophenweg 12, D-69120 Heidelberg, Germany

²⁹Humboldt-Universität zu Berlin, Institut für Physik, Newtonstrasse 15, D-12489 Berlin, Germany

³⁰Imperial College London, London, SW7 2AZ, United Kingdom

³¹University of Iowa, Iowa City, Iowa 52242, USA

³²Iowa State University, Ames, Iowa 50011-3160, USA

³³Johns Hopkins University, Baltimore, Maryland 21218, USA

- ³⁴Laboratoire de l'Accélérateur Linéaire, IN2P3/CNRS et Université Paris-Sud 11, Centre Scientifique d'Orsay, B. P. 34, F-91898 Orsay Cedex, France
- ³⁵Lawrence Livermore National Laboratory, Livermore, California 94550, USA
- ³⁶University of Liverpool, Liverpool L69 7ZE, United Kingdom
- ³⁷Queen Mary, University of London, London, E1 4NS, United Kingdom
- ³⁸University of London, Royal Holloway and Bedford New College, Egham, Surrey TW20 0EX, United Kingdom
- ³⁹University of Louisville, Louisville, Kentucky 40292, USA
- ⁴⁰Johannes Gutenberg-Universität Mainz, Institut für Kernphysik, D-55099 Mainz, Germany
- ⁴¹University of Manchester, Manchester M13 9PL, United Kingdom
- ⁴²University of Maryland, College Park, Maryland 20742, USA
- ⁴³University of Massachusetts, Amherst, Massachusetts 01003, USA
- ⁴⁴Massachusetts Institute of Technology, Laboratory for Nuclear Science, Cambridge, Massachusetts 02139, USA
- ⁴⁵McGill University, Montréal, Québec, Canada H3A 2T8
- ^{46a}INFN Sezione di Milano, I-20133 Milano, Italy
- ^{46b}Dipartimento di Fisica, Università di Milano, I-20133 Milano, Italy
- ⁴⁷University of Mississippi, University, Mississippi 38677, USA
- ⁴⁸Université de Montréal, Physique des Particules, Montréal, Québec, Canada H3C 3J7
- ⁴⁹Mount Holyoke College, South Hadley, Massachusetts 01075, USA
- ^{50a}INFN Sezione di Napoli, I-80126 Napoli, Italy
- ^{50b}Dipartimento di Scienze Fisiche, Università di Napoli Federico II, I-80126 Napoli, Italy
- ⁵¹NIKHEF, National Institute for Nuclear Physics and High Energy Physics, NL-1009 DB Amsterdam, The Netherlands
- ⁵²University of Notre Dame, Notre Dame, Indiana 46556, USA
- ⁵³The Ohio State University, Columbus, Ohio 43210, USA
- ⁵⁴University of Oregon, Eugene, Oregon 97403, USA
- ^{55a}INFN Sezione di Padova, I-35131 Padova, Italy
- ^{55b}Dipartimento di Fisica, Università di Padova, I-35131 Padova, Italy
- ⁵⁶Laboratoire de Physique Nucléaire et de Hautes Energies, IN2P3/CNRS, Université Pierre et Marie Curie-Paris6, Université Denis Diderot-Paris7, F-75252 Paris, France
- ⁵⁷University of Pennsylvania, Philadelphia, Pennsylvania 19104, USA
- ^{58a}INFN Sezione di Perugia, I-06100 Perugia, Italy
- ^{58b}Dipartimento di Fisica, Università di Perugia, I-06100 Perugia, Italy
- ^{59a}INFN Sezione di Pisa, I-56127 Pisa, Italy
- ^{59b}Dipartimento di Fisica, Università di Pisa, I-56127 Pisa, Italy
- ^{59c}Scuola Normale Superiore di Pisa, I-56127 Pisa, Italy
- ⁶⁰Princeton University, Princeton, New Jersey 08544, USA
- ^{61a}INFN Sezione di Roma, I-00185 Roma, Italy
- ^{61b}Dipartimento di Fisica, Università di Roma La Sapienza, I-00185 Roma, Italy
- ⁶²Universität Rostock, D-18051 Rostock, Germany
- ⁶³Rutherford Appleton Laboratory, Chilton, Didcot, Oxon, OX11 0QX, United Kingdom
- ⁶⁴CEA, Irfu, SPP, Centre de Saclay, F-91191 Gif-sur-Yvette, France
- ⁶⁵SLAC National Accelerator Laboratory, Stanford, California 94309 USA
- ⁶⁶University of South Carolina, Columbia, South Carolina 29208, USA
- ⁶⁷Stanford University, Stanford, California 94305-4060, USA
- ⁶⁸State University of New York, Albany, New York 12222, USA
- ⁶⁹Tel Aviv University, School of Physics and Astronomy, Tel Aviv, 69978, Israel
- ⁷⁰University of Tennessee, Knoxville, Tennessee 37996, USA
- ⁷¹University of Texas at Austin, Austin, Texas 78712, USA
- ⁷²University of Texas at Dallas, Richardson, Texas 75083, USA
- ^{73a}INFN Sezione di Torino, I-10125 Torino, Italy
- ^{73b}Dipartimento di Fisica Sperimentale, Università di Torino, I-10125 Torino, Italy

*Deceased.

†Present address: Temple University, Philadelphia, PA 19122, USA.

‡Also at Università di Perugia, Dipartimento di Fisica, Perugia, Italy.

§Also at Università di Roma La Sapienza, I-00185 Roma, Italy.

||Present address: University of South Alabama, Mobile, AL 36688, USA.

¶Also at Laboratoire de Physique Nucléaire et de Hautes Energies, IN2P3/CNRS, Université Pierre et Marie Curie-Paris6, Université Denis Diderot-Paris7, F-75252 Paris, France.

**Also at Università di Sassari, Sassari, Italy.

^{74a}*INFN Sezione di Trieste, I-34127 Trieste, Italy*^{74b}*Dipartimento di Fisica, Università di Trieste, I-34127 Trieste, Italy*⁷⁵*IFIC, Universitat de Valencia-CSIC, E-46071 Valencia, Spain*⁷⁶*University of Victoria, Victoria, British Columbia, Canada V8W 3P6*⁷⁷*Department of Physics, University of Warwick, Coventry CV4 7AL, United Kingdom*⁷⁸*University of Wisconsin, Madison, Wisconsin 53706, USA*

(Received 2 February 2010; published 19 May 2010)

A search for the $Z(3930)$ resonance in $\gamma\gamma$ production of the $D\bar{D}$ system has been performed using a data sample corresponding to an integrated luminosity of 384 fb^{-1} recorded by the *BABAR* experiment at the PEP-II asymmetric-energy electron-positron collider. The $D\bar{D}$ invariant mass distribution shows clear evidence of the $Z(3930)$ state with a significance of 5.8σ . We determine mass and width values of $(3926.7 \pm 2.7 \pm 1.1) \text{ MeV}/c^2$ and $(21.3 \pm 6.8 \pm 3.6) \text{ MeV}$, respectively. A decay angular analysis provides evidence that the $Z(3930)$ is a tensor state with positive parity and C parity ($J^{PC} = 2^{++}$); therefore we identify the $Z(3930)$ state as the $\chi_{c2}(2P)$ meson. The value of the partial width $\Gamma_{\gamma\gamma} \times \mathcal{B}(Z(3930) \rightarrow D\bar{D})$ is found to be $(0.24 \pm 0.05 \pm 0.04) \text{ keV}$.

DOI: 10.1103/PhysRevD.81.092003

PACS numbers: 13.66.Bc, 14.40.Lb, 13.25.Gv

I. INTRODUCTION

Interest in the field of charmonium spectroscopy has been renewed with the recent discovery of numerous charmonium and charmoniumlike states [1–11]. However, very little is known about the first radially excited $\chi_{cJ}(2P)$ states which are expected to exist in the mass region from 3.9 to 4.0 GeV/c^2 , just above the $D\bar{D}$ threshold [12]. The Belle Collaboration has observed the $Z(3930)$ state in $\gamma\gamma$ production of the $D\bar{D}$ system [13], and this is considered a strong candidate for the $\chi_{c2}(2P)$ state; indeed it is so labeled in Ref. [14]. The Belle analysis obtained a mass of $m = (3929 \pm 5 \pm 2) \text{ MeV}/c^2$ and a total width of $\Gamma = (29 \pm 10 \pm 2) \text{ MeV}$, with quantum numbers $J^{PC} = 2^{++}$ preferred. The partial width $\Gamma_{\gamma\gamma} \times \mathcal{B}(Z(3930) \rightarrow D\bar{D})$ was determined as $(0.18 \pm 0.05 \pm 0.03) \text{ keV}$, where $\Gamma_{\gamma\gamma}$ is the radiative width of the $Z(3930)$ state, under the assumption that $J = 2$. The observation of this state has not been confirmed so far [14].

In this paper the process $\gamma\gamma \rightarrow D\bar{D}$, illustrated by the Feynman diagram shown in Fig. 1, is studied in a search for the $Z(3930)$ state. In Fig. 1, the initial state positron, e^+ (electron, e^-), emits the virtual photon γ_1^* (γ_2^*), yielding the final state positron, $e^{+'}$ (electron, $e^{-'}$); the momentum transfer to γ_1^* (γ_2^*) is q_1 (q_2). The virtual photons interact to produce the $D\bar{D}$ final state. When the $e^{+'}$ and the $e^{-'}$ are emitted along the beam directions the values of q_1^2 and q_2^2 are predominantly close to zero, and the two photons can be considered to be quasireal. Since in this case neither the $e^{+'}$ nor the $e^{-'}$ is detected, the analysis is termed *untagged*.

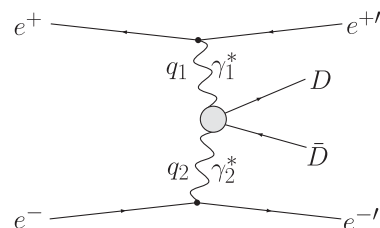
The data sample used in this analysis corresponds to an integrated luminosity of 384 fb^{-1} recorded at the $Y(4S)$ resonance (10.58 GeV) and at a center of mass (c.m.) energy of 10.54 GeV by the *BABAR* detector at the PEP-II asymmetric-energy e^+e^- collider.

The *BABAR* detector is described briefly in Sec. II, and the principal criteria used in the selection of candidate two-photon-interaction events are discussed in Sec. III. The

reconstruction of $D\bar{D}$ pair events is presented in Sec. IV, and the relevant Monte Carlo simulations are detailed in Sec. V. The purity and reconstruction efficiency of the $\gamma\gamma \rightarrow D\bar{D}$ event sample are considered in Secs. VI and VII, respectively, and the $D\bar{D}$ signal yield and invariant mass resolution are presented in Sec. VIII; the mass and total width for the $Z(3930)$ state are obtained from a fit to the $D\bar{D}$ invariant mass distribution. The angular distribution in the $D\bar{D}$ rest frame for the $Z(3930)$ mass region is studied in Sec. IX, and the implications for the spin of the $Z(3930)$ state are discussed. In Sec. X the partial radiative width of the $Z(3930)$ state is extracted. Sources of systematic uncertainty are detailed in Sec. XI, and the results of the analysis are summarized in Sec. XII.

II. THE *BABAR* DETECTOR

The *BABAR* detector is described in detail elsewhere [15]. Charged particles are detected, and their momenta measured, with a combination of five layers of double-sided silicon microstrip detectors (SVT) and a 40-layer cylindrical drift chamber (DCH), both coaxial with the cryostat of a superconducting solenoidal magnet which produces a magnetic field of 1.5 T. Charged-particle identification is achieved by measurements of the energy loss dE/dx in the tracking devices and by means of an internally reflecting, ring-imaging Cherenkov detector (DIRC). Photons and electrons are detected and their energies mea-

FIG. 1. Two-photon production of the $D\bar{D}$ system.

sured with a CsI(Tl) electromagnetic calorimeter (EMC), covering 90% of the 4π solid angle in the $\Upsilon(4S)$ rest frame. The instrumented flux return of the magnetic field is used to identify muons and K_L^0 .

III. SELECTION OF TWO-PHOTON-INTERACTION EVENTS

The selection of two-photon-interaction events for an untagged analysis is based on established procedures (see for instance Refs. [16,17]). Because of the small scattering angles involved, most of the incoming beam energy is carried away by the e^{+} and e^{-} (see Fig. 1). This results in a large value of the missing mass squared

$$m_{\text{miss}}^2 = (p_{e^+} + p_{e^-} - p_D - p_{\bar{D}})^2, \quad (1)$$

where p_{e^\pm} are the four-momenta of the beam electron and positron and $p_D, p_{\bar{D}}$ are the four-momenta of the final state D and \bar{D} mesons, respectively. In addition, for these events, the resultant transverse momentum of the $D\bar{D}$ system $p_t(D\bar{D})$ is limited to small values.

In order to establish selection criteria for $\gamma\gamma \rightarrow D\bar{D}$ events, the reaction

$$e^+e^- \rightarrow K^+K^-\pi^+\pi^-X \quad (2)$$

is studied first using a data sample corresponding to an integrated luminosity of 235 fb^{-1} . The system X contains no additional charged particles. This reaction has been

chosen because it has the same particle configuration as one of the final states we consider in this analysis. The charged kaons and pions are identified as described in detail in Sec. IV. Neutral pions are reconstructed from pairs of photons with deposited energy in the EMC larger than 100 MeV. It is required that no π^0 meson candidate be found in a selected event.

Two-photon production of the $K^-K^+\pi^+\pi^-$ system should yield large values of m_X^2 , the missing mass squared,

$$m_X^2 = (p_{e^+} + p_{e^-} - p_{K^+} - p_{K^-} - p_{\pi^+} - p_{\pi^-})^2. \quad (3)$$

In addition, production of the $K^-K^+\pi^+\pi^-$ system via initial state radiation (ISR) should yield the small values of m_X^2 associated with the ISR photon, for which detection is not required. The observed distribution of the $K^-K^+\pi^+\pi^-$ invariant mass, $m(K^-K^+\pi^+\pi^-)$, resulting from the reaction of Eq. (2) is shown in Fig. 2(a).

There are clear signals corresponding to the production of $\eta_c(1S)$, $\chi_{c0}(1P)$, and $\chi_{c2}(1P)$, and, since these states all have positive C parity, it is natural to associate them with two-photon production. Similarly, the large J/ψ signal observed would be expected to result from ISR production, because of the negative C parity of the J/ψ . For the parameters of these states, see Table I.

The distribution of m_X^2 for $2.8 \leq m(K^-K^+\pi^+\pi^-) \leq 3.8 \text{ GeV}/c^2$ is shown in Fig. 2(b). The large peak near zero is interpreted as being due mainly to ISR production

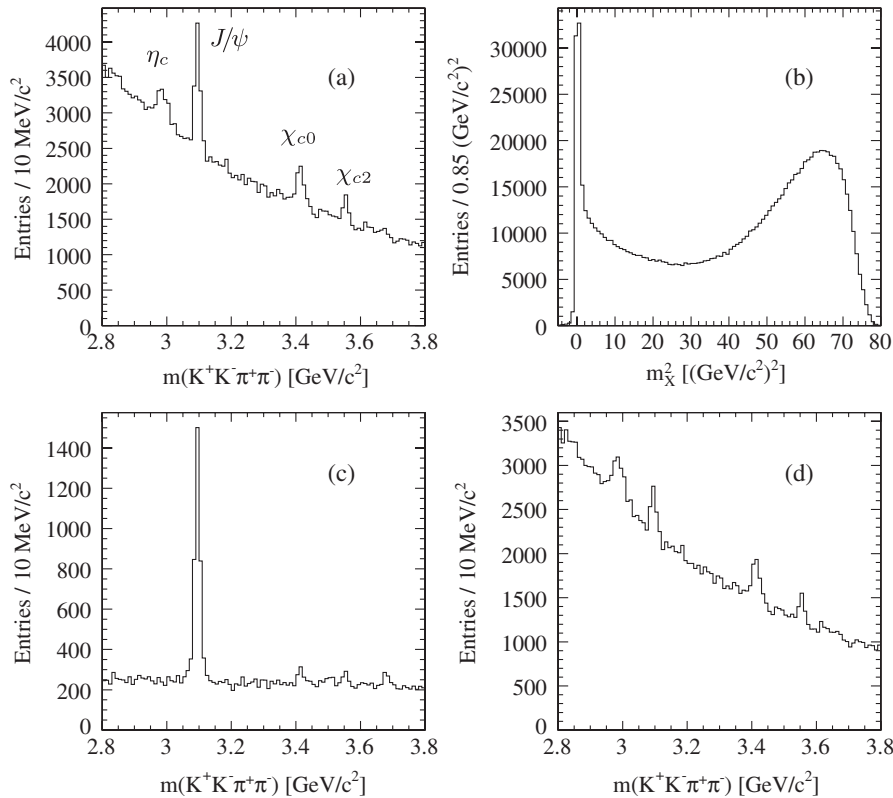


FIG. 2. (a) $K^+K^-\pi^+\pi^-$ mass distribution for all events without any requirement on m_X^2 ; (b) corresponding m_X^2 distribution; (c) $m(K^+K^-\pi^+\pi^-)$ with the requirement $m_X^2 < 10 \text{ (GeV}/c^2)^2$; (d) $m(K^+K^-\pi^+\pi^-)$ with the requirement $m_X^2 > 10 \text{ (GeV}/c^2)^2$.

TABLE I. Charmonium states observed in the $e^+e^- \rightarrow K^+K^-\pi^+\pi^-X$ test data sample [14].

	Mass (MeV/ c^2)	J^{PC}
$\eta_c(1S)$	(2980.3 ± 1.2)	0^{-+}
$J/\psi(1S)$	(3096.916 ± 0.011)	1^{--}
$\chi_{c0}(1P)$	(3414.75 ± 0.31)	0^{++}
$\chi_{c1}(1P)$	(3510.66 ± 0.07)	1^{++}
$\chi_{c2}(1P)$	(3556.20 ± 0.09)	2^{++}
$\eta_c(2S)$	(3637 ± 4)	0^{-+}
$\psi(2S)$	(3686.09 ± 0.04)	1^{--}

of the $K^-K^+\pi^+\pi^-$ system, while two-photon-production events would be expected to occur at larger values of m_X^2 . This is shown explicitly by the distributions of Figs. 2(c) and 2(d), which correspond to the requirements $m_X^2 < 10$ (GeV/ c^2)² and $m_X^2 > 10$ (GeV/ c^2)², respectively.

In Fig. 2(c) there is a large J/ψ signal, and a much smaller $\psi(2S)$ signal can also be seen. For e^+e^- collisions at a c.m. energy of 10.58 GeV, the ISR production cross section for J/ψ is about 3 times larger than for $\psi(2S)$; also $\mathcal{B}(J/\psi \rightarrow K^-K^+\pi^+\pi^-)$ is approximately 9 times larger than the corresponding $\psi(2S)$ branching fraction value [14].

It follows that the observed J/ψ signal would be expected to be ≈ 27 times larger than that for $\psi(2S)$. The signals in Fig. 2(c) seem to be consistent with this expectation, and they are also in agreement with the detailed analysis of ISR production of the $K^-K^+\pi^+\pi^-$ system in Ref. [18]. There is a $\chi_{c2}(1P)$ signal in Fig. 2(c) which is comparable in size to the $\psi(2S)$ signal. The branching fraction for $\psi(2S) \rightarrow K^-K^+\pi^+\pi^-$ is $\approx 7.5 \times 10^{-4}$ [14], while the product $\mathcal{B}(\psi(2S) \rightarrow \gamma\chi_{c2}(1P)) \times \mathcal{B}(\chi_{c2}(1P) \rightarrow K^-K^+\pi^+\pi^-)$ is $\approx 7.8 \times 10^{-4}$ [14], so that the presence of such a $\chi_{c2}(1P)$ signal is consistent with the expected transition rates. For the $\chi_{c1}(1P)$, $\mathcal{B}(\psi(2S) \rightarrow \gamma\chi_{c1}(1P)) \times \mathcal{B}(\chi_{c1}(1P) \rightarrow K^-K^+\pi^+\pi^-) \approx 4.0 \times 10^{-4}$, and so a $\chi_{c1}(1P)$ signal of approximately half the size of the $\chi_{c2}(1P)$ signal would be expected in Fig. 2(c); again the data seem to be in reasonable agreement with this expectation.

Finally, for the $\chi_{c0}(1P)$, $\mathcal{B}(\psi(2S) \rightarrow \gamma\chi_{c0}(1P)) \times \mathcal{B}(\chi_{c0}(1P) \rightarrow K^-K^+\pi^+\pi^-) \approx 16.8 \times 10^{-4}$, and the corresponding signal in Fig. 2(c) would be expected to be about twice the size of the $\psi(2S)$ signal. The $\chi_{c0}(1P)$ signal seems to be larger than that of the $\psi(2S)$, but not by a factor of 2; this may be because the larger energy photon from the $\psi(2S) \rightarrow \gamma\chi_{c0}(1P)$ transition, when combined with the ISR photon, can yield a value of m_X^2 which is larger than 10 (GeV/ c^2)². In summary, the signals observed in Fig. 2(c) appear consistent with those expected for an ISR-production mechanism, especially since there is no indication of any remnant of the large $\eta_c(1S)$ of Fig. 2(a). Furthermore, the χ_{cJ} signals in Fig. 2(c) are removed by requiring that the transverse momentum of

the $K^-K^+\pi^+\pi^-$ system be less than 50 MeV/ c [see discussion of Fig. 2(d) below], which indicates clearly that they do not result from two-photon production.

In Fig. 2(d), the $\eta_c(1S)$ signal of Fig. 2(a) appears to have survived the $m_X^2 > 10$ (GeV/ c^2)² requirement in its entirety, and the $\chi_{c0}(1P)$ and $\chi_{c2}(1P)$ signals have been reduced slightly, as discussed in the previous paragraph; in both Figs. 2(a) and 2(d) there is some indication of a small signal in the region of the $\eta_c(2S)$ mass. A J/ψ signal of about one-third of that in Fig. 2(a) is present also in Fig. 2(d). This is interpreted as being primarily due to (a) the emission of more than one initial state photon, with the consequence that values of m_X^2 greater than 10 (GeV/ c^2)² are obtained, (b) the ISR production of the $\psi(2S)$ with subsequent decay to J/ψ + neutrals, and (c) two-photon production of the $\chi_{c2}(1P)$ followed by $\chi_{c2}(1P) \rightarrow \gamma J/\psi$, which has a 20% branching fraction [14].

It follows from the above that the requirement $m_X^2 > 10$ (GeV/ c^2)² significantly reduces ISR contributions to the $K^-K^+\pi^+\pi^-$ final state while leaving signals associated with two-photon production essentially unaffected. For this reason, the requirement that m_{miss}^2 of Eq. (1) be greater than 10 (GeV/ c^2)² is chosen as a principal selection criterion for the isolation of events corresponding to $\gamma\gamma \rightarrow D\bar{D}$.

As mentioned above, it is expected that for an untagged analysis of $\gamma\gamma \rightarrow D\bar{D}$, the transverse momentum $p_t(D\bar{D})$ should be small. In order to quantify this statement, the data of Fig. 2(d) were divided into intervals of 50 MeV/ c in the transverse momentum of the $K^-K^+\pi^+\pi^-$ system with respect to the e^+e^- collision axis, which is considered also to be the collision axis for two-photon-production events. For each interval a fit was made to the $m(K^-K^+\pi^+\pi^-)$ mass distribution in the mass region $2.7 \leq m(K^-K^+\pi^+\pi^-) \leq 3.3$ GeV/ c^2 . The function used consists of a second-order polynomial to describe the background, a Gaussian function for the J/ψ signal, and a Breit-Wigner for the $\eta_c(1S)$ signal convolved with a Gaussian to account for the resolution. The p_t dependence of the resulting $\eta_c(1S)$ yield is shown in Fig. 3(a), and that of the J/ψ yield is shown in Fig. 3(b). The shapes of the distributions are quite similar for $p_t > 100$ MeV/ c , but the interval from 50–100 MeV/ c contains ≈ 180 more $\eta_c(1S)$ signal events, and that for 0–50 MeV/ c exhibits an excess of ≈ 800 signal events. This behavior is expected for two-photon production of the $\eta_c(1S)$. Thus, the requirement $p_t(D\bar{D}) < 50$ MeV/ c is imposed as the second principal selection criterion for the extraction of $\gamma\gamma \rightarrow D\bar{D}$ events.

Since the two-photon reactions $\gamma\gamma \rightarrow K^-K^+\pi^+\pi^-$ and $\gamma\gamma \rightarrow D\bar{D}$ are quasiexclusive in the sense that only the final state particles e^+ and e^- are undetected it is required in both instances that the total energy deposits E_{EMC} in the EMC which are unmatched to any charged-particle track be less than 400 MeV. The net effect is a small reduction in

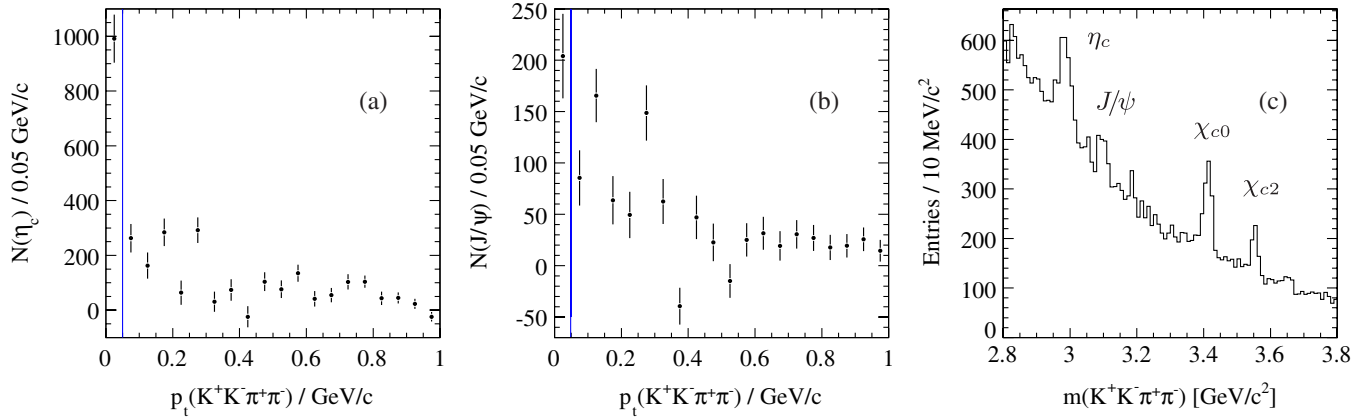


FIG. 3 (color online). Signal yield dependence on $p_t(K^+K^-\pi^+\pi^-)$ for (a) $\eta_c(1S)$ and (b) J/ψ . The vertical lines mark the $p_t(K^+K^-\pi^+\pi^-) < 0.05 \text{ MeV}/c$ region for selecting two-photon events. (c) Resulting $K^+K^-\pi^+\pi^-$ mass distribution after applying the principal selection criteria discussed in Sec. III.

the smooth background. The histogram of Fig. 3(c) corresponds to the $K^+K^-\pi^+\pi^-$ candidates of Fig. 2(d) after requiring $p_t(K^+K^-\pi^+\pi^-) < 50 \text{ MeV}/c$ and that the EMC energy sum be less than 400 MeV. The p_t criterion reduces the $\eta_c(1S)$ signal by a factor ≈ 2 , while the J/ψ signal is reduced by a factor ≈ 5 , as is the continuum background at 2.7 GeV/c^2 . More significantly, the continuum background at 3.7 GeV/c^2 , just below the $D\bar{D}$ threshold, is reduced by a factor ≈ 10 .

It follows that the net effect of the three principal selection criteria described above [missing mass $m_{\text{miss}}^2 > 10 (\text{GeV}/c^2)^2$, resultant transverse momentum $p_t(D\bar{D}) < 50 \text{ MeV}/c$, and total energy deposit in the calorimeter $E_{\text{EMC}} < 400 \text{ MeV}$] is to significantly enhance the number of two-photon-production events relative to the events resulting from ISR production, continuum production, and combinatoric background.

Concerning the histogram of Fig. 3(c), the product $\Gamma_{\gamma\gamma}(\eta_c(1S)) \times \mathcal{B}(\eta_c(1S) \rightarrow K^+K^-\pi^+\pi^-)$ is 1.7 ± 1.0 times that for the $\chi_{c0}(1P)$ state [14], and in Fig. 3(c) the $\eta_c(1S)$ signal contains ≈ 950 events [cf. the 0–50 MeV/c interval of Fig. 3(a)], while the $\chi_{c0}(1P)$ signal contains ≈ 550 events. It follows that the signal sizes agree well with the ratio expected on the basis of a two-photon production mechanism. In a similar vein, the ratio of the partial width $\Gamma_{\gamma\gamma}(\chi_{cJ}) \times \mathcal{B}(\chi_{cJ} \rightarrow K^+K^-\pi^+\pi^-)$ for $\chi_{c0}(1P)$ and $\chi_{c2}(1P)$ is 9 ± 2 [14], so that after taking into account the $(2J+1)$ spin factors, the signals observed in Fig. 3(c) would be expected to be approximately in the ratio 1.8 ± 0.4 . The $\chi_{c2}(1P)$ signal contains ≈ 200 events, and so is consistent with this expectation.

IV. RECONSTRUCTION OF $D\bar{D}$ EVENTS

Candidate $D\bar{D}$ events are reconstructed in the five combinations of D decay modes listed in Table II (the use of charge conjugate states is implied throughout the text).

Events are selected by requiring the exact number of charged-particle tracks defined by the relevant final state.

Track selection requirements include transverse momentum $p_t > 0.1 \text{ GeV}/c$, at least 12 coordinate measurements in the DCH, a maximum distance of closest approach (DOCA) of 1.5 cm to the z axis, with this point at a maximum DOCA of 10 cm to the xy plane at $z = 0$.

Kaon candidates are identified based on the normalized kaon, pion, and proton likelihood values (L_K , L_π , and L_p) obtained from the particle identification system, by requiring $L_K/(L_K + L_\pi) > 0.9$ and $L_K/(L_K + L_p) > 0.2$. Tracks that fulfill $L_K/(L_K + L_\pi) < 0.82$ and $L_p/(L_p + L_\pi) < 0.98$ are selected as pions. Additionally, in both cases the track should be inconsistent with electron identification.

Photon candidates are selected when their deposited energy in the EMC is larger than 100 MeV. Neutral pions are reconstructed from pairs of photons with combined mass within $[0.115, 0.155] \text{ GeV}/c^2$ and a π^0 mass constraint is applied to them.

The D candidate decay products are fitted to a common vertex with a D meson mass constraint applied; candidates with a χ^2 fit probability greater than 0.1% are retained. Accepted $D\bar{D}$ pairs are refitted to a common vertex consistent with the e^+e^- interaction region, and those with a χ^2 fit probability $p_v(D\bar{D})$ greater than 0.1% are retained.

TABLE II. D decay final states studied in this analysis; for channels N5, N6, and N7, inclusion of the corresponding charge conjugate combination is implied.

Channel	D decay mode	\bar{D} decay mode	
N4	$D^0 \bar{D}^0$	$D^0 \rightarrow K^-\pi^+$	$\bar{D}^0 \rightarrow K^+\pi^-$
N5	$D^0 \bar{D}^0$	$D^0 \rightarrow K^-\pi^+$	$\bar{D}^0 \rightarrow K^+\pi^-\pi^0$
N6	$D^0 \bar{D}^0$	$D^0 \rightarrow K^-\pi^+$	$\bar{D}^0 \rightarrow K^+\pi^-\pi^-\pi^+$
N7	$D^0 \bar{D}^0$	$D^0 \rightarrow K^-\pi^+\pi^+\pi^-$	$\bar{D}^0 \rightarrow K^+\pi^-\pi^0$
C6	$D^+ D^-$	$D^+ \rightarrow K^-\pi^+\pi^+$	$D^- \rightarrow K^+\pi^-\pi^-$

TABLE III. Summary of selection criteria used for identifying $D\bar{D}$ candidates.

Channel	No. of π^0	D mass window (MeV/ c^2)	\bar{D} mass window (MeV/ c^2)
N4	0	1863.4 ± 22	1863.4 ± 22
N5	1	1863.4 ± 22	1863.4 ± 43
N6	0	1863.4 ± 22	1863.4 ± 16
N7	1	1863.4 ± 16	1863.4 ± 43
C6	0	1868.5 ± 18	1868.5 ± 18

TABLE IV. Summary of requirements used for selecting only $D\bar{D}$ candidates from two-photon events. These criteria are identical for all decay modes.

Channel	m_{miss}^2 (GeV/ c^2) ²	$p_i(D\bar{D})$ (GeV/ c)	E_{EMC} (GeV)
All modes	>10.0	<0.05	<0.4

Events with π^0 candidates other than those from a D or \bar{D} decay of interest are rejected. These preselection criteria are identical for all five combinations of D decay modes.

The signal regions for accepted, unconstrained D candidates are then fitted using a multi-Gaussian signal function

$$R(m) = \int_{\sigma_0}^{r\sigma_0} \frac{1}{r\sigma^2} e^{-(m-m_0)^2/2\sigma^2} d\sigma \quad (4)$$

with free parameters σ_0 , r (minimal and maximal width) and m_0 ; the background is described by a polynomial. The full width at half maximum (FWHM) of the signal line shape in data is used to define each D signal region; D candidates are selected from a region of width ± 1.5 FWHM around the mean mass. The mass windows are listed in Table III.

From the list of accepted $D\bar{D}$ candidates those produced in two-photon events are then selected by applying the three criteria defined in Sec. III (summarized in Table IV). These criteria are also identical for all combinations of D decay modes.

Depending on the decay mode, up to 2.5% of the events have multiple candidates which passed all selection criteria. In this case, the candidate with the best fit probability $p_i(D\bar{D})$ is chosen. Based on Monte Carlo (MC) studies, the correct candidate is selected in more than 99% of the cases with this method.

The resulting invariant mass spectra for D meson candidates after all selection criteria have been applied are shown in Fig. 4 for events in which the mass of the recoil \bar{D}

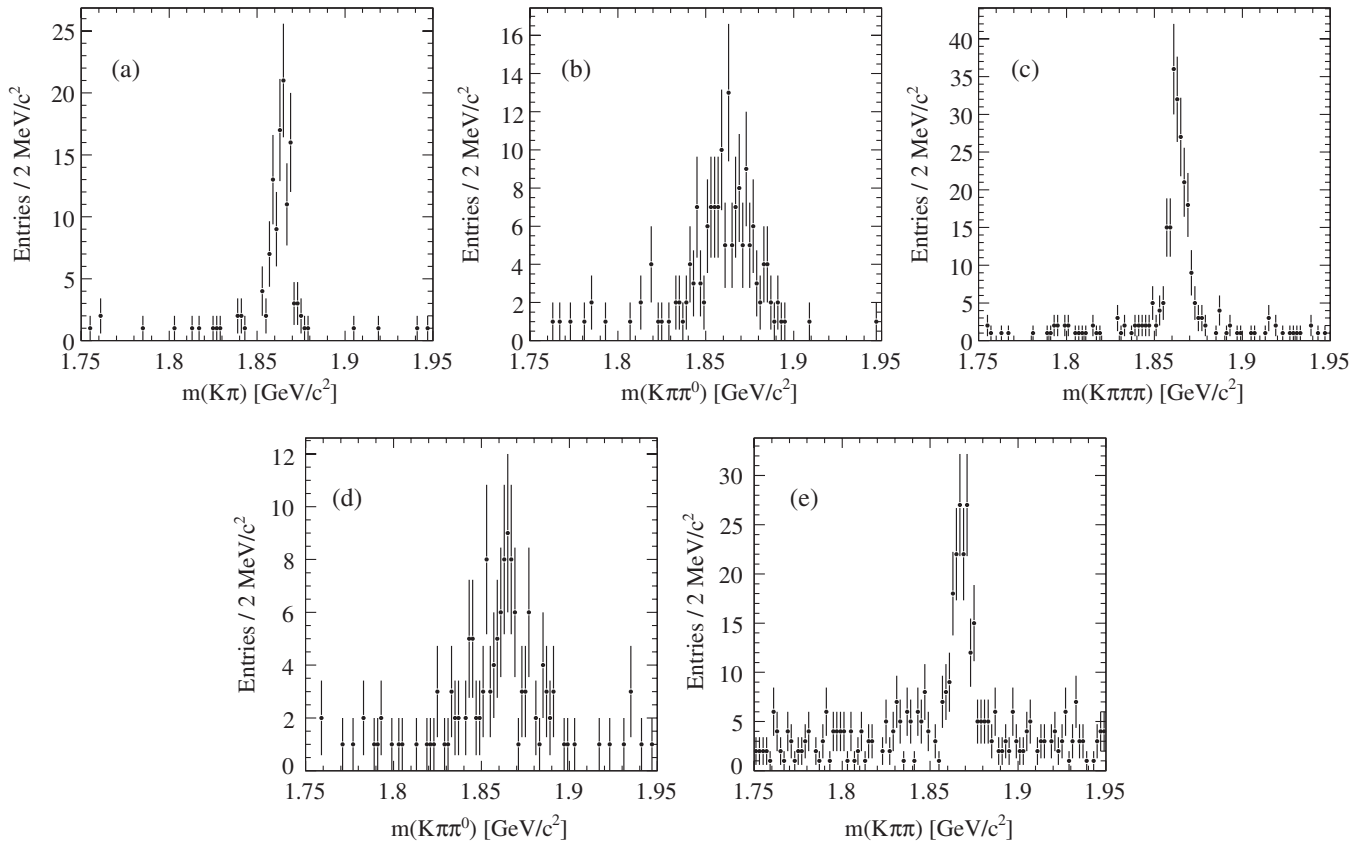


FIG. 4. Candidate D invariant mass distributions after all selection criteria. The mass of the accompanying \bar{D} candidate is required to lie within its signal region as defined in Table III. (a) $K^- \pi^+$ in N4; (b) $K^+ \pi^- \pi^0$ in N5; (c) $K^- \pi^+ \pi^+ \pi^-$ in N6; (d) $K^+ \pi^- \pi^0$ in N7; (e) $K^- \pi^+ \pi^+$ in C6.

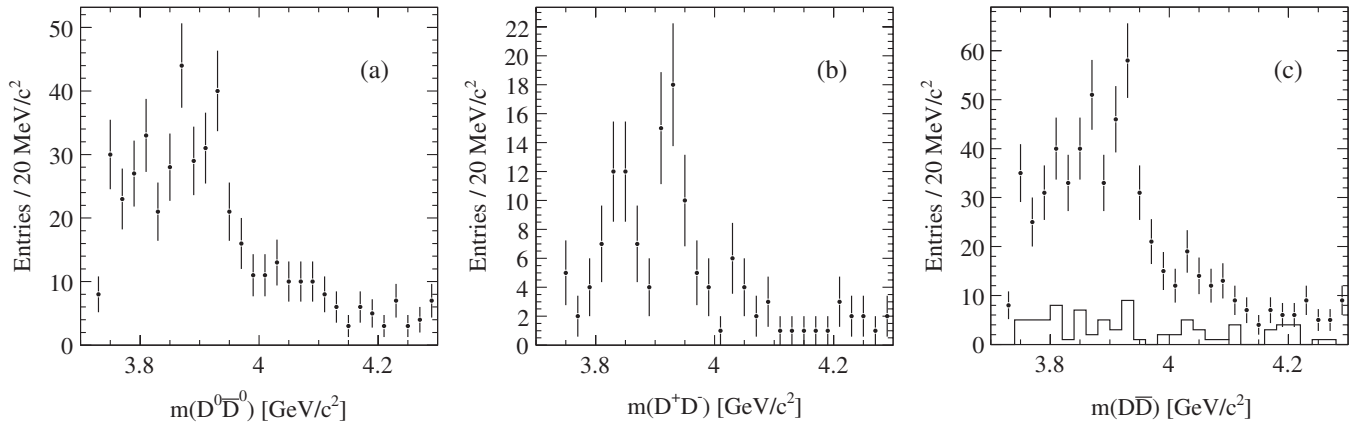


FIG. 5. $D\bar{D}$ invariant mass distribution for the (a) $D^0\bar{D}^0$ and (b) D^+D^- channels. (c) The combined $D\bar{D}$ invariant mass distribution. The open histogram in (c) shows the combinatoric background estimated from the D -mass sidebands.

candidate lies within the defined signal region. In all modes, clear signals with small backgrounds are obtained. The resulting $D\bar{D}$ invariant mass distributions are shown in Figs. 5(a) and 5(b) for the neutral modes (N4, N5, N6, N7), and for the charged mode (C6), respectively. The combined spectrum is shown in Fig. 5(c). An enhancement near $3.93 \text{ GeV}/c^2$ is visible.

To estimate the amount of combinatoric background in the signal region, the two-dimensional space spanned by the invariant masses of the D and \bar{D} candidates is divided into nine regions: one central signal region and eight sideband regions above and below the signal region as shown in Fig. 6 for the $K^-\pi^+\pi^-/K^+\pi^-\pi^-$ (C6) mode. The mass range for the signal region is ± 1.5 FWHM around the mean mass. The sideband regions are 1.5 FWHM wide, leaving a gap of 1.5 FWHM between signal and sideband. No significant contribution from combinatoric background is observed in the $D\bar{D}$ spectrum [Fig. 5(c)].

An attempt was made to isolate the signal in Fig. 5(c) by a weighting method. This assumes that signal and background events have different angular distributions, and was

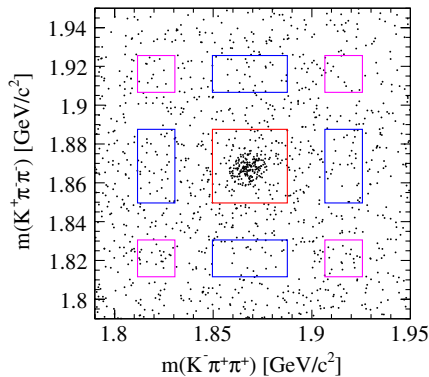


FIG. 6 (color online). $K^+\pi^-\pi^-$ mass vs $K^-\pi^+\pi^+$ mass for the channel C6 of Table II. The boxes correspond to the signal and sideband regions.

successfully used in a previous *BABAR* analysis [19]. Simulations with a $J^{PC} = 2^{++}$ signal (generated with its correct angular distribution) plus background showed that the method works well with high signal statistics and moderate background, but is not reliable with the limited statistics and background of the current analysis. Therefore, the method was not considered further in the present analysis.

V. MONTE CARLO STUDIES

For modeling the detector resolution, efficiency studies and the estimation of the two-photon width $\Gamma_{\gamma\gamma}$ of the resonance, MC events were generated which pass the same reconstruction and analysis chain as the experimental data. For each signal decay channel about 10^6 events were generated. Additional events were generated for background modes involving D^* mesons. The GAMGAM two-photon event generator was used to simulate $\gamma\gamma \rightarrow Z(3930) \rightarrow D\bar{D}$ events, while the decays of the D and \bar{D} mesons were generated by EVTGEN [20]. The detector response was simulated using the GEANT4 [21] package. The program GAMGAM uses the formalism suggested by Budnev, Ginzburg, Meledin, and Serbo (BGMS) [22]. It was developed for CLEO and was used, for example, in the analysis of $\chi_{c0}(1P)$, $\chi_{c2}(1P) \rightarrow 4\pi$ decays [23]. GAMGAM was later adapted to *BABAR* and used for the analysis of $\eta_c(1S, 2S) \rightarrow K_S^0 K^\pm \pi^\mp$ [16].

For small photon virtualities $|q_{1,2}|^2$ (see Fig. 1) the differential cross section for the process $e^+e^- \rightarrow e^+e^-\gamma\gamma$, $\gamma\gamma \rightarrow X$ is given by the product $L \times F \times \sigma(\gamma\gamma \rightarrow X)$, where L is the two-photon flux. The form factor F extrapolates the process to virtual photons and is *a priori* not known. A plausible model

$$F = \left(\frac{1}{1 - q_1^2/m_v^2} \right)^2 \times \left(\frac{1}{1 - q_2^2/m_v^2} \right)^2 \quad (5)$$

is used [24], with m_v being the mass of an appropriate

vector boson (ρ , J/ψ , Z^0). In the calculations relevant to this analysis $m_v = m(J/\psi)$ was used, as the $Z(3930)$ is expected to be a charmonium state. An alternative model was used in order to evaluate systematic uncertainties associated with MC simulations (see Sec. XI).

To validate the GAMGAM generator its output was compared to that of another two-photon generator (TREPS) used by Belle [25]. The cross sections for the reactions $e^+e^- \rightarrow e^+e^-\gamma\gamma$, $\gamma\gamma \rightarrow \eta_c(1S, 2S)$ were calculated in GAMGAM and compared to the Belle values [26]. In order to compare the different generators, the cross sections were calculated using the hypothetical values $\Gamma_{\gamma\gamma} \times \mathcal{B}(\eta_c(1S, 2S) \rightarrow \text{final state}) = 1$ keV, and $q_{1,2}^2$ was restricted to values smaller than 1 $(\text{GeV}/c^2)^2$. The TREPS results were 2.11 pb for $\eta_c(1S)$ and 0.86 pb for $\eta_c(2S)$. The corresponding GAMGAM values were 2.13 and 0.84 pb, respectively. The two generators are in agreement at the level of a few percent.

For a global check, the cross sections for the continuum reaction $e^+e^- \rightarrow e^+e^-\gamma\gamma$, $\gamma\gamma \rightarrow \mu^+\mu^-$ were calculated with GAMGAM for various c.m. energies and compared to QED predictions [27,28], which describe the data with high accuracy [29]. Here, the agreement was slightly worse, due to the imperfect tuning of the GAMGAM program for these reactions. Similar results were obtained when checking against calculations with nonrelativistic models for $\eta_c(1S)$ and $\chi_{c2}(1P)$ [30]. Nevertheless this comparison showed that GAMGAM works properly under these conditions also. These studies lead to the assignment of a total systematic uncertainty of $\pm 3\%$ associated with the MC simulation (see Sec. XI).

VI. PURITY OF THE $\gamma\gamma \rightarrow D\bar{D}$ SAMPLE

The selection criteria used to enhance the two-photon content of the $D\bar{D}$ sample were discussed in Sec. III. They were developed by investigating the reaction $e^+e^- \rightarrow K^+K^-\pi^+\pi^-X$ of Eq. (2). Figure 3(c) shows that after the selection procedure the signals associated with $\gamma\gamma$ reactions, like that for the $\eta_c(1S)$, are enhanced, while signals such as that for the J/ψ , which are typical of ISR production, are suppressed. The $p_t(D\bar{D})$ distribution is shown in Fig. 7 for events in the $Z(3930)$ signal region, defined as the region from 3.91 to 3.95 GeV/c^2 . Here the $p_t(D\bar{D})$ selection criterion has not been applied. The data are fitted with a curve for $\gamma\gamma$ events obtained from MC, plus a linear background derived from sideband studies of the $D\bar{D}$ mass spectrum. The fit indicates that the majority of $D\bar{D}$ candidates in the signal region result from two-photon interactions.

VII. RECONSTRUCTION EFFICIENCY

The reconstruction efficiency for each decay mode is calculated as a function of $m(D\bar{D})$ using MC events which pass the same reconstruction and selection criteria as real

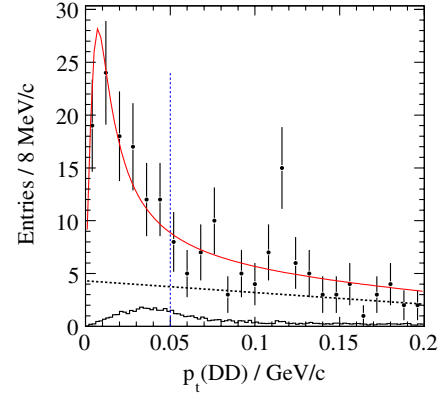


FIG. 7 (color online). Distribution of $p_t(D\bar{D})$ for data in the $Z(3930)$ signal region. The fitted line shape consists of the expected $\gamma\gamma$ line shape obtained from MC plus a linear background (dotted line). The vertical line shows the p_t criterion for selecting $\gamma\gamma$ events. The histogram shows the shape of the $p_t(D\bar{D})$ distribution from simulated $D^*\bar{D}$ events with missing π^0 or γ . The bump in this distribution is not seen in the data distribution, indicating that any $D^*\bar{D}$ background is small.

events and includes detector acceptance, track reconstruction, and particle identification efficiencies. The mass-dependent efficiency $\epsilon_i(m(D\bar{D}))$ for each channel i is fitted with a polynomial in $m(D\bar{D})$ and is found to decrease with increasing $D\bar{D}$ mass. For the combination of modes [Fig. 5(c)], an overall weighted efficiency $\epsilon^B(m(D\bar{D}))$, which includes the branching fractions for the D decays, is computed using

$$\epsilon^B(m(D\bar{D})) = \frac{5}{2} \frac{\sum_{i=1}^5 N_i(m(D\bar{D}))}{\sum_{i=1}^5 \frac{N_i(m(D\bar{D}))}{\epsilon_i^B(m(D\bar{D}))}}, \quad (6)$$

as was done in Ref. [31]; $N_i(m(D\bar{D}))$ is the number of $D\bar{D}$ candidates in the data mass spectrum for channel i , and $\epsilon_i^B(m(D\bar{D}))$ is defined as the product of the efficiency ϵ_i as parametrized by the fitted polynomial and the branching fraction \mathcal{B}_i for the i th channel, as follows:

$$\epsilon_i^B(m(D\bar{D})) = \epsilon_i(m(D\bar{D})) \times \mathcal{B}_i. \quad (7)$$

The factor $\frac{1}{2}$ originates from referring to $D\bar{D}$ ($D^0\bar{D}^0$ and D^+D^-) events, and the factor 5 from summing over the five channels. Figure 8 shows the mass dependence of $\epsilon^B(m(D\bar{D}))$, which is parametrized by a straight line. The large uncertainties are due to the limited statistics available in the data samples. The error bars do not contain the uncertainties in the branching fractions; these will be discussed separately in Sec. XI in the context of systematic error estimation. The data are weighted by this mean efficiency, which is scaled by a constant value d to obtain weights near 1,

$$\epsilon(m(D\bar{D})) = d \times \epsilon^B(m(D\bar{D})) \quad (8)$$

as weights far from 1 might result in incorrect errors for the

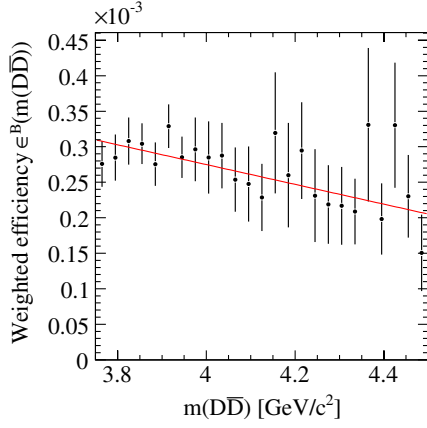


FIG. 8 (color online). Mass dependence of the weighted reconstruction efficiency calculated using Eq. (6), described by a straight line.

signal yield obtained in the maximum likelihood fit [32]. The resulting $D\bar{D}$ mass distribution will be discussed in Sec. VIII.

VIII. DETECTOR RESOLUTION AND SIGNAL YIELD

Monte Carlo events are used for the calculation of the mass-dependent detector resolution. The mass resolution is determined by studying the difference between the reconstructed and the generated $D\bar{D}$ mass (Δm_{res}). As an example, the distribution for channel C6 is shown in Fig. 9(a). A good description of the distribution is obtained using a multi-Gaussian fit [Eq. (4)]. The parameters r and $\sigma_0(m(D\bar{D}))$ were determined for every decay channel. The variation of $\sigma_0(m(D\bar{D}))$, which is parametrized by a second-order polynomial, and of the width (FWHM) of the resolution function with increasing mass are shown in Figs. 9(b) and 9(c). For channel C6, $r = 5.380 \pm 0.137$ and $\sigma_0(m(D\bar{D})) = (-0.038 + 0.018m - 0.002m^2) \text{ GeV}/c^2$, where $m(D\bar{D})$ is given in units of

GeV/c^2 . The distributions of Fig. 9 are well described by the fitted curves shown. Comparing the generated $Z(3930)$ mass with the reconstructed MC value shows that the latter is systematically low by about $0.9 \text{ MeV}/c^2$, independently of the fit model. This effect is observed both in the combined fit and in fits to the individual channels. The measured J/ψ mass in the $K^+K^-\pi^+\pi^-$ test sample (Sec. III) differs by the same value from the world average [14]; this offset has been seen in other $\gamma\gamma$ studies at *BABAR* [16] as well. Accordingly, the mass value obtained from the fit to data will be corrected by $+0.9 \text{ MeV}/c^2$. This offset value will also be used as a conservative estimate of the systematic uncertainty in the mass scale. The difference between the generated and reconstructed decay width values amounts to 0.14 MeV , and is discussed in Sec. XI with respect to systematic error estimation.

In order to describe the signal structure in data around $3.93 \text{ GeV}/c^2$ a relativistic Breit-Wigner function $BW(m)$ is used, where

$$BW(m) = \left(\frac{p_m}{p_{m_0}}\right)^{2L+1} \left(\frac{m_0}{m}\right) \frac{F_r^2}{(m_0^2 - m^2)^2 + \Gamma_m^2 m_0^2} \quad (9)$$

with m_0 as the nominal mass of the resonance; the Blatt-Weisskopf coefficients F_r for different angular momentum values L are given by

$$F_r(L=0) = 1, \quad (10)$$

$$F_r(L=1) = \frac{\sqrt{1 + (Rp_{m_0})^2}}{\sqrt{1 + (Rp_m)^2}}, \quad (11)$$

$$F_r(L=2) = \frac{\sqrt{9 + 3(Rp_{m_0})^2 + (Rp_{m_0})^4}}{\sqrt{9 + 3(Rp_m)^2 + (Rp_m)^4}}, \quad (12)$$

and the value

$$R = 1.5 (\text{GeV}/c)^{-1}$$

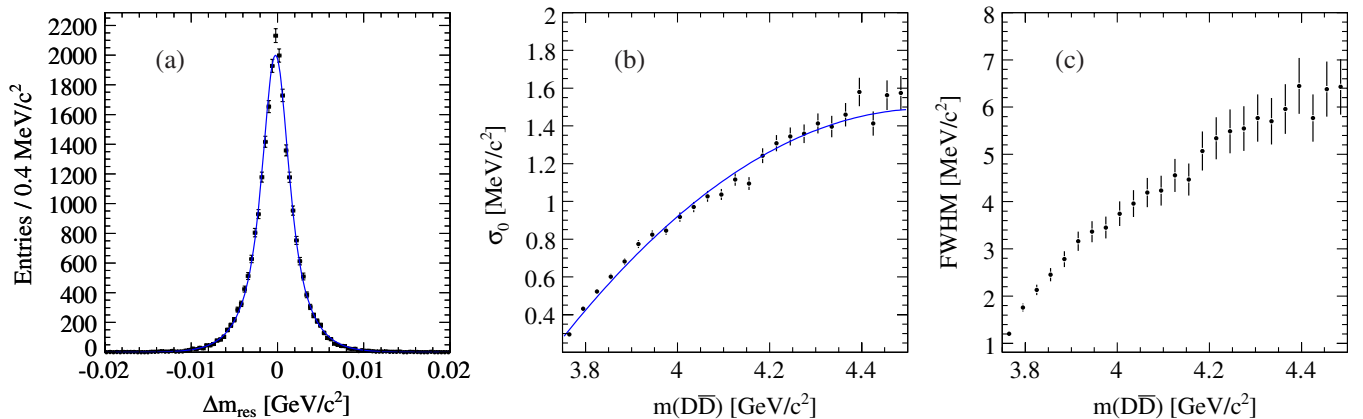


FIG. 9 (color online). (a) Detector resolution Δm_{res} for channel C6; the fitted curve is described in the text; (b) mass dependence of the resolution function parameter σ_0 ; (c) mass dependence of the FWHM of the resolution function.

is used, corresponding to the value given in Ref. [33]. The mass-dependent width is given by

$$\Gamma_m = \Gamma_r \left(\frac{p_m}{p_{m_0}} \right)^{2L+1} \left(\frac{m_0}{m} \right) F_r^2 \quad (13)$$

with Γ_r the total width of the resonance. Here the existence of other possible decay modes is ignored. The momentum of a given D candidate in the $D\bar{D}$ center of mass frame is denoted by p_m ; p_{m_0} is the corresponding value for $m = m_0$. In the standard fit, spin $J = 2$ ($L = 2$) is chosen on the basis of the angular distribution analysis described in Sec. IX.

The signal function is convolved with the mass- and decay-mode-dependent resolution model parametrized as discussed previously in this section. The background is parametrized by the function

$$D(m) \propto \sqrt{m^2 - m_t^2} (m - m_t)^\alpha \exp[-\beta(m - m_t)] \quad (14)$$

which takes the $D\bar{D}$ threshold m_t into account. In the lower mass region, the line shape does not describe the background exactly. Other functional forms were tried (Sec. XI), but no improvement was obtained. The data and the curves which result from the standard ($J = 2$) fit are shown in Fig. 10.

From the unbinned maximum likelihood fit to the five mass spectra the $Z(3930)$ values $m_0 = (3925.8 \pm 2.7)$ MeV/ c^2 and $\Gamma_r = (21.3 \pm 6.8)$ MeV are obtained for the mass and total width, respectively (all errors in this section are statistical only). The mass is corrected by +0.9 MeV/ c^2 as described above, resulting in a final mass value of (3926.7 ± 2.7) MeV/ c^2 . The efficiency-corrected yield amounts to $N = (76 \pm 17)$ signal events. This value is based on weights around 1 as discussed in Sec. VII; taking the constant used to scale the efficiency into account [see Eq. (8)], this corresponds to a total $Z(3930)$ signal of $N_{e^B} = (285 \pm 64) \times 10^3$ events.

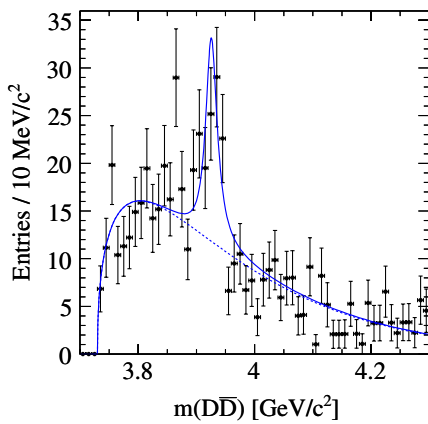


FIG. 10 (color online). Efficiency-corrected mean $D\bar{D}$ mass distribution with standard fit. The dashed curve shows the background line shape (see Sec. VIII).

The statistical significance of the peak is 5.8σ and is derived from the difference $\Delta \ln \mathcal{L}$ between the negative logarithmic likelihood of the nominal fit and that of a fit where the parameter for the signal yield is fixed to zero. This is then used to evaluate a p value:

$$p = \int_{2\Delta \ln \mathcal{L}}^{\infty} f(z; n_d) dz, \quad (15)$$

where $f(z; n_d)$ is the χ^2 probability density function and n_d is the number of degrees of freedom, 3 in this case. We then determine the equivalent one-dimensional significance from this p value.

IX. ANGULAR DISTRIBUTION AND SPIN OF THE $Z(3930)$ STATE

General conservation laws limit the possibilities for the J^{PC} values of the $Z(3930)$ state. For two-photon production the initial state has positive C parity and hence the final state must have positive C parity also. For the $D\bar{D}$ final state, $C = (-1)^{L+S} = (-1)^L$ since the total spin S is zero. Positive C parity then implies that the $D\bar{D}$ system must have orbital angular momentum L which is even, and hence have even parity. It follows that for the $Z(3930)$ state $J^{PC} = J^{++}$ with $J = 0, 2, 4, \dots$. In order to investigate the possible values of J , we have compared the decay angular distribution measured in the $Z(3930)$ signal region to the distributions expected for $J = 0$ and $J = 2$; higher spin values are very unlikely for a state only 200 MeV/ c^2 above threshold.

The decay angle θ is defined as the angle of the D meson in the $D\bar{D}$ system relative to the $D\bar{D}$ lab momentum vector. Figure 11 shows the $Z(3930)$ signal yield obtained from fits to the $D\bar{D}$ mass spectrum for ten regions of $|\cos\theta|$. The data have been weighted by a $\cos\theta$ -dependent efficiency, which was determined in a similar manner as described in Sec. VII for the mass-dependent efficiency (Fig. 12). In these fits, the mass and width of the resonance have been

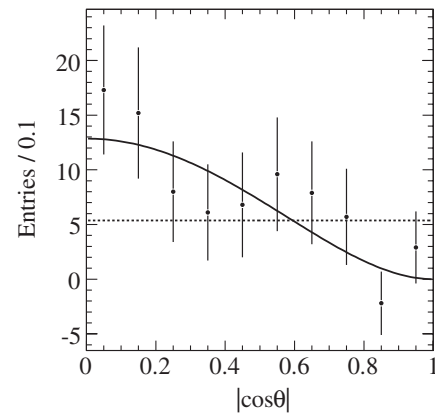


FIG. 11. Signal yield as a function of $|\cos\theta|$ derived from fits to the efficiency-corrected $D\bar{D}$ spectrum. The solid curve is the expected distribution for spin 2 with dominating helicity-2 contribution, the dotted straight line is for spin 0.

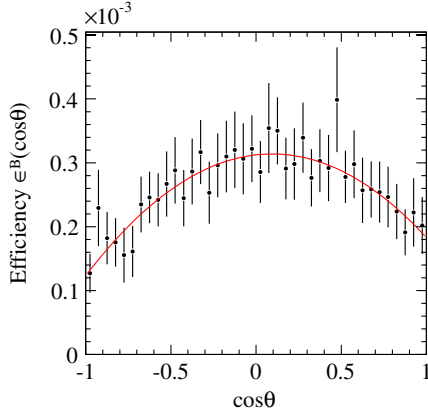


FIG. 12 (color online). Angular dependence of the weighted reconstruction efficiency $\epsilon^B(\cos\theta)$ based on Eq. (6), described by a second-order polynomial.

fixed to the values found in Sec. VIII, and Eq. (14) has been used to describe the background. Other background models have been tried, obtaining distributions fully consistent with Fig. 11.

The function describing the decay angular distribution for spin 2 has been calculated using the helicity formalism and has the form

$$\frac{dN}{d\cos\theta} \propto \sin^4\theta. \quad (16)$$

It has been assumed that the dominating amplitude has helicity 2. This is in agreement with previous measurements [34] and theoretical predictions [24,30]. The distribution of Eq. (16) was fitted to the experimental angular

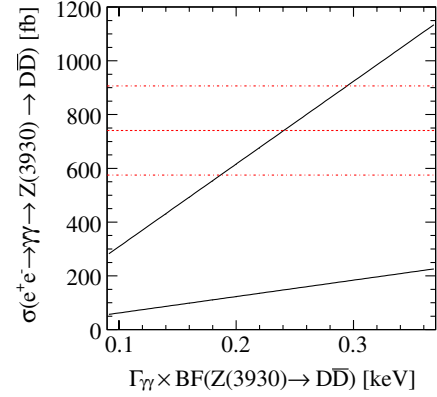


FIG. 13 (color online). Dependence of the cross section $\sigma(e^+e^- \rightarrow \gamma\gamma \rightarrow Z(3930) \rightarrow D\bar{D})$ on the two-photon width $\Gamma_{\gamma\gamma} \times \mathcal{B}(Z(3930) \rightarrow D\bar{D})$, calculated with the two-photon generator GAMGAM. The upper solid line is for spin 2, while the lower solid line is for spin 0. The measured value (horizontal dashed line) and its uncertainty range (horizontal dot-dashed lines) are indicated.

distribution, and a χ^2/NDF value of 5.63/9 was obtained, with NDF indicating the number of degrees of freedom. For a flat distribution, which is expected for spin 0, a $\chi^2/\text{NDF} = 15.55/9$ was obtained. It follows that the preferred J^{PC} assignment is 2^{++} .

X. TWO-PHOTON WIDTH OF THE Z(3930) STATE

From the efficiency-corrected number of observed signal events, N_{ϵ^B} , we determine the total experimental cross section

$$\sigma_{\text{exp}}(e^+e^- \rightarrow e^+e^- \gamma\gamma, \gamma\gamma \rightarrow Z(3930), Z(3930) \rightarrow D\bar{D}) = N_{\epsilon^B} / \int \mathcal{L} dt = 741 \pm 166 \text{ fb}, \quad (17)$$

where the integrated luminosity for the data sample analyzed is $\int \mathcal{L} dt = (384 \pm 4) \text{ fb}^{-1}$ and the error is only statistical.

On the other hand, the cross section for Z(3930) production is given by

$$\sigma(e^+e^- \rightarrow \gamma\gamma, \gamma\gamma \rightarrow Z(3930)) = L \times F \times \sigma(\gamma\gamma \rightarrow Z(3930)) \quad (18)$$

with

$$\sigma(\gamma\gamma \rightarrow Z(3930)) = \int 4\pi(2J+1)(\hbar c)^2 10^{-6} m_Z^3 \frac{\Gamma_{\gamma\gamma}}{\sqrt{K}m} \frac{\Gamma_{\text{tot}}}{(m_Z^2 - m^2)^2 + m_Z^2 \Gamma_{\text{tot}}^2} dm^2 \quad (19)$$

and can be calculated using GAMGAM. Here L is the two-photon flux, F is the form factor (see Sec. V), m_Z (Γ_{tot}) is the resonance mass (width), and $\Gamma_{\gamma\gamma}$ is the two-photon width of the resonance. The kinematical factor K is given by $K = (q_1 q_2)^2 - q_1^2 q_2^2$ (q_i represent four vectors of photons). Further information can be found in Refs. [22,24,35]. The cross section depends on the spin of the resonance and on $\Gamma_{\gamma\gamma}$. It is plotted for $J = 2$ and $J = 0$ in Fig. 13 as a function of $\Gamma_{\gamma\gamma}$. From a comparison to

the experimental cross section [Eq. (17)], the partial width $\Gamma_{\gamma\gamma} \times \mathcal{B}(Z(3930) \rightarrow D\bar{D})$ is found to have the value $(0.24 \pm 0.05) \text{ keV}$ when $J = 2$ is chosen as the most probable spin value (see Sec. IX).

XI. SYSTEMATIC ERROR ESTIMATION

Several sources of systematic uncertainty have been considered for the mass, decay width, and signal yield of the Z(3930) state. The yield determines the value of

TABLE V. Results of the systematic uncertainty studies for the mass, decay width, and efficiency-corrected signal yield of the $Z(3930)$ state. Listed are the differences with respect to the standard values. $\Delta(\Gamma_{\gamma\gamma} \times \mathcal{B})$ numbers are given for spin $J = 2$ only. For the combined error, the values are added in quadrature.

Source of systematic uncertainty	$\Delta m(Z(3930))$ (MeV/ c^2)	$\Delta\Gamma(Z(3930))$ (MeV)	$\Delta(\Gamma_{\gamma\gamma} \times \mathcal{B})$ (keV)
Choice of spin $J = 1, J = 0$	<0.05	<0.05	...
Value of R (Breit-Wigner)	<0.05	<0.05	<0.0005
Background $D'(m)$	0.4	3.0	0.029
Fit precision and mass scale	0.9	0.1	0.001
Convolution steps = 35	0.2	0.2	0.003
Convolution range +0.02 MeV/ c^2	<0.05	0.9	0.003
Resolution multi-Gauss $r \pm \delta r$	<0.05	0.1	<0.0005
Combined reconstr. efficiency: polynomial	<0.05	0.4	<0.0005
Tracking efficiency correction	<0.05	<0.05	0.022
π^0 efficiency correction	<0.05	<0.05	0.003
Error in D branching fractions	<0.05	<0.05	0.010
Efficiency: angular distribution	0.018
Generator precision	0.007
Choice of form factor	0.002
PID	0.4	1.8	0.004
Uncertainty in D mass	0.3
Luminosity	0.002
Combined error	± 1.1	± 3.6	± 0.04

$\Gamma_{\gamma\gamma} \times \mathcal{B}(Z(3930) \rightarrow D\bar{D})$. The standard fit to the efficiency-corrected mass spectrum is repeated with appropriate modifications. The differences Δ between the results obtained and the standard results are used as estimates of systematic uncertainty. No correlations have been taken into account. The results are summarized in Table V. Deviations for the mass ($|\Delta m|$), total width ($|\Delta\Gamma|$), and two-photon width [$|\Delta(\Gamma_{\gamma\gamma} \times \mathcal{B})|$] are considered negligible if they are less than 0.05 MeV/ c^2 , 0.05 MeV, and 0.0005 keV, respectively.

A. Fit parametrization

Signal line shape.—The standard fit has assumed spin $J = 2$ for the resonance (Sec. VIII). Using different spin values and R values has no significant impact on the results [Table V; $\Delta(\Gamma_{\gamma\gamma} \times \mathcal{B})$ numbers are given for spin $J = 2$ only].

Background description.—Different parametrizations of the background in the $m(D\bar{D})$ distribution have been used. Besides the nominal background [Eq. (14)], the following background shape was tried:

$$D'(m) \propto \left(1 - \exp\left[\frac{-(m - \alpha)}{\beta}\right]\right) \left(\frac{m}{\alpha}\right)^\beta + \gamma \left(\frac{m}{\alpha} - 1\right); \quad (20)$$

the fit had a slightly worse, but still acceptable, likelihood value. The mass value changes by $\Delta m = +0.4$ MeV/ c^2 , the width by $\Delta\Gamma = +3.0$ MeV, the signal yield by +9 events with respect to the standard fit, and $\Gamma_{\gamma\gamma} \times \mathcal{B}$ changes accordingly by +0.029 keV (Table V). Other

background models yield consistent estimates for this source of systematic uncertainty.

B. Detector resolution

Fit precision and mass scale.—A fit of the convolution of signal line shape and resolution model to the MC sample has been performed. The mass offset observed in MC has been included by correcting the mass value by +0.9 MeV/ c^2 . As a conservative estimate, this number is also used as the systematic uncertainty for the mass scale. The deviation between the generated width and the value obtained from the fit is 0.14 MeV, and again this is used as a conservative estimate of systematic uncertainty. Based on the uncertainty of the width, a value of $\Delta\Gamma_{\gamma\gamma} \times \mathcal{B} = 0.001$ keV is derived.

Resolution model.—The parameters of the multi-Gaussian resolution model were modified. The number of steps was enlarged from 25 to 35, the total convolution range for each data point enlarged by +0.02 MeV/ c^2 , and the parameter r of the multi-Gaussian was varied within its fit uncertainty δr . The corresponding shifts in the mass are $\Delta m = +0.2, <0.05, \text{ and } <0.05$ MeV/ c^2 . For $\Delta\Gamma$, shifts of $-0.2, -0.9, \text{ and } -0.1$ MeV are obtained; from the modified signal yield, shifts of $-0.003, -0.003, \text{ and } <0.0005$ keV were obtained for $\Gamma_{\gamma\gamma} \times \mathcal{B}$ (Table V).

C. Combined reconstruction efficiency

Parametrization.—The average mass-dependent reconstruction efficiency has been parametrized by a straight line in the standard fit (Fig. 8). Using a fit with a second-

order polynomial, the width changes by -0.4 MeV; no mass shift was observed with respect to the standard fit result. For the signal yield, $+1$ entry is obtained; this yields no significant shift for $\Gamma_{\gamma\gamma} \times \mathcal{B}$ (Table V).

Tracking and neutrals correction.—For the tracking efficiency a correction by -0.8% is applied per charged-particle track. This gives a correction factor of 0.968 for modes N4, N5, and 0.953 for N6, N7, and C6. The systematic uncertainty assigned to the tracking efficiency is 1.4% per track for decays with more than 5 charged-particle tracks and 1.3% otherwise. The resulting uncertainty for $\Gamma_{\gamma\gamma} \times \mathcal{B}$ is 0.022 keV. Concerning efficiency corrections for neutral particles, a correction factor of 0.984 with an uncertainty of 3% per π^0 is used for modes N5 and N7. The resulting uncertainty for $\Gamma_{\gamma\gamma} \times \mathcal{B}$ is 0.003 keV (Table V).

Uncertainty on the D branching fractions.—The errors on the D branching fractions have been taken into account by varying the values of \mathcal{B}_i used in Eq. (6) within their standard deviations. No significant change is observed in mass and decay width. For the two-photon width $\Delta(\Gamma_{\gamma\gamma} \times \mathcal{B}) = \pm 0.010$ keV is obtained (Table V).

Effect of angular distribution on efficiency.—The MC data sample used to obtain the efficiency and resolution was generated with a flat distribution in $\cos\theta$. To estimate the effect of the angular distribution on the reconstruction efficiency, a MC sample described by a $\sin^4\theta$ distribution has been generated and reconstructed. Comparing these reconstructed data with the nominal MC sample, the mean efficiencies differ by 8%, relatively, resulting in $\Delta(\Gamma_{\gamma\gamma} \times \mathcal{B}) = \pm 0.018$ keV.

D. Cross-section calculation from GAMGAM

Precision.—In Sec. V a relative uncertainty of $\pm 3\%$ was obtained for the calculated cross section. Propagating this error into the calculation of $\Gamma_{\gamma\gamma} \times \mathcal{B}$, an uncertainty $\Delta(\Gamma_{\gamma\gamma} \times \mathcal{B}) = \pm 0.007$ keV results.

Form factor.—In the standard analysis the form factor of Eq. (5) has been used with $m_v = m(J/\psi)$. In order to estimate potential systematic effects, the cross section was evaluated using a model predicted by perturbative QCD [36]

$$F = \frac{1}{(1 - q_1^2/m_v^2 - q_2^2/m_v^2)^2}. \quad (21)$$

The cross section calculated with GAMGAM does not increase significantly ($\approx 0.1\%$) compared to that obtained using Eq. (5). Simultaneously the experimental efficiency decreases by 1%, so that the net effect on $\Gamma_{\gamma\gamma} \times \mathcal{B}$ is small. Similar effects have been observed when data and calculations with and without q^2 selection criteria are compared [25,26,37], and also in a previous CLEO analysis [38]. As a result a systematic uncertainty of $\pm 1\%$ is attributed to form factor uncertainty and this yields a deviation $\Delta(\Gamma_{\gamma\gamma} \times \mathcal{B}) = \pm 0.002$ keV.

E. Other uncertainties

Particle identification (PID).—For PID studies, the pion selection criteria have been tightened significantly, and the efficiency has been recalculated accordingly. The fit to the mass spectrum yields a change of -0.4 MeV/ c^2 for the mass and -1.8 MeV for the width. For $\Delta(\Gamma_{\gamma\gamma} \times \mathcal{B})$ a change of -0.004 keV results.

D mass uncertainty.—The uncertainty of the D meson mass is taken into account. Both for D^0 and D^\pm , the uncertainty is 0.17 MeV/ c^2 [14], which results in an uncertainty of ± 0.34 MeV/ c^2 in the mass of the $Z(3930)$ state.

Integrated luminosity uncertainty.—For the integrated luminosity, an uncertainty of $\pm 1\%$ is assigned. From this an uncertainty $\Delta(\Gamma_{\gamma\gamma} \times \mathcal{B}) = \pm 0.002$ keV is obtained.

F. Total systematic uncertainty

The systematic uncertainty estimates discussed in Secs. XI A, XI B, XI C, XI D, and XI E are summarized in Table V. The individual estimates are combined in quadrature to yield net systematic uncertainty estimates on the $Z(3930)$ mass, total width, and value of $\Gamma_{\gamma\gamma} \times \mathcal{B}(Z(3930) \rightarrow D\bar{D})$ of 1.1 MeV/ c^2 , 3.6 MeV, and 0.04 keV, respectively, as reported on the last line of Table V.

XII. SUMMARY

In the $\gamma\gamma \rightarrow D\bar{D}$ reaction a signal in the $D\bar{D}$ mass spectrum has been observed near 3.93 GeV/ c^2 with a significance of 5.8σ which agrees with the observation of the $Z(3930)$ resonance by the Belle Collaboration [13]. The mass and total width of the $Z(3930)$ state are measured to be $(3926.7 \pm 2.7(\text{stat}) \pm 1.1(\text{syst}))$ MeV/ c^2 and $(21.3 \pm 6.8(\text{stat}) \pm 3.6(\text{syst}))$ MeV, respectively.

The production and decay mechanisms allow only positive parity and C parity, and an analysis of the $Z(3930)$ decay angular distribution favors a tensor over a scalar interpretation. The preferred assignment for spin and parity of the $Z(3930)$ state is therefore $J^{PC} = 2^{++}$. The product of the branching fraction to $D\bar{D}$ times the two-photon width of the $Z(3930)$ state is measured to be $\Gamma_{\gamma\gamma} \times \mathcal{B}(Z(3930) \rightarrow D\bar{D}) = (0.24 \pm 0.05(\text{stat}) \pm 0.04(\text{syst}))$ keV, assuming spin $J = 2$. The parameters obtained are consistent with the Belle results, and with the expectations for the $\chi_{c2}(2P)$ state.

ACKNOWLEDGMENTS

We are grateful for the extraordinary contributions of our PEP-II colleagues in achieving the excellent luminosity and machine conditions that have made this work possible. The success of this project also relies critically on the expertise and dedication of the computing organizations that support *BABAR*. The collaborating institutions wish to thank SLAC for its support and the kind hospitality

extended to them. This work is supported by the U.S. Department of Energy and National Science Foundation, the Natural Sciences and Engineering Research Council (Canada), the Commissariat à l'Énergie Atomique and Institut National de Physique Nucléaire et de Physique des Particules (France), the Bundesministerium für Bildung und Forschung and Deutsche Forschungsgemeinschaft (Germany), the Istituto Nazionale di Fisica

Nucleare (Italy), the Foundation for Fundamental Research on Matter (The Netherlands), the Research Council of Norway, the Ministry of Education and Science of the Russian Federation, Ministerio de Educación y Ciencia (Spain), and the Science and Technology Facilities Council (United Kingdom). Individuals have received support from the Marie-Curie IEF program (European Union) and the A. P. Sloan Foundation.

-
- [1] S.-K. Choi *et al.* (Belle Collaboration), *Phys. Rev. Lett.* **91**, 262001 (2003).
- [2] B. Aubert *et al.* (BABAR Collaboration), *Phys. Rev. D* **71**, 071103 (2005).
- [3] D. Acosta *et al.* (CDF II Collaboration), *Phys. Rev. Lett.* **93**, 072001 (2004).
- [4] V.M. Abazov *et al.* (D0 Collaboration), *Phys. Rev. Lett.* **93**, 162002 (2004).
- [5] K. Abe *et al.* (Belle Collaboration), *Phys. Rev. Lett.* **98**, 082001 (2007).
- [6] S.-K. Choi *et al.* (Belle Collaboration), *Phys. Rev. Lett.* **94**, 182002 (2005).
- [7] B. Aubert *et al.* (BABAR Collaboration), *Phys. Rev. Lett.* **101**, 082001 (2008).
- [8] B. Aubert *et al.* (BABAR Collaboration), *Phys. Rev. Lett.* **95**, 142001 (2005).
- [9] C.-Z. Yuan *et al.* (Belle Collaboration), *Phys. Rev. Lett.* **99**, 182004 (2007).
- [10] B. Aubert *et al.* (BABAR Collaboration), *Phys. Rev. Lett.* **98**, 212001 (2007).
- [11] X.-L. Wang *et al.* (Belle Collaboration), *Phys. Rev. Lett.* **99**, 142002 (2007).
- [12] S. Godfrey and N. Isgur, *Phys. Rev. D* **32**, 189 (1985).
- [13] S. Uehara *et al.* (Belle Collaboration), *Phys. Rev. Lett.* **96**, 082003 (2006).
- [14] C. Amsler *et al.* (Particle Data Group), *Phys. Lett. B* **667**, 1 (2008), and 2009 partial update for the 2010 edition.
- [15] B. Aubert *et al.* (BABAR Collaboration), *Nucl. Instrum. Methods Phys. Res., Sect. A* **479**, 1 (2002).
- [16] B. Aubert *et al.* (BABAR Collaboration), *Phys. Rev. Lett.* **92**, 142002 (2004).
- [17] B. Aubert *et al.* (BABAR Collaboration), *Phys. Rev. D* **79**, 092001 (2009).
- [18] B. Aubert *et al.* (BABAR Collaboration), *Phys. Rev. D* **76**, 012008 (2007).
- [19] B. Aubert *et al.* (BABAR Collaboration), *Phys. Rev. D* **78**, 034008 (2008).
- [20] D. Lange, *Nucl. Instrum. Methods Phys. Res., Sect. A* **462**, 152 (2001).
- [21] S. Agostinelli *et al.* (GEANT4 Collaboration), *Nucl. Instrum. Methods Phys. Res., Sect. A* **506**, 250 (2003).
- [22] V.M. Budnev *et al.*, *Phys. Rep.* **15**, 181 (1975).
- [23] B.I. Eisenstein *et al.* (CLEO Collaboration) *Phys. Rev. Lett.* **87**, 061801 (2001).
- [24] M. Poppe, *Int. J. Mod. Phys. A* **1**, 545 (1986).
- [25] S. Uehara, KEK Report No. 96-11 H, 1996.
- [26] S. Uehara *et al.* (Belle Collaboration), *Eur. Phys. J. C* **53**, 1 (2007).
- [27] F. A. Berends *et al.*, *Phys. Lett. B* **148**, 489 (1984).
- [28] F. A. Berends *et al.*, *Nucl. Phys.* **B253**, 441 (1985).
- [29] B. Adeva *et al.*, *Phys. Rev. Lett.* **48**, 721 (1982).
- [30] G. A. Schuler *et al.*, *Nucl. Phys.* **B523**, 423 (1998).
- [31] B. Aubert *et al.* (BABAR Collaboration), *Phys. Rev. D* **76**, 111105 (2007).
- [32] A. G. Frodesen *et al.*, *Probability and Statistics in Particle Physics* (Universitetsforlaget, Bergen, Norway, 1979).
- [33] F. von Hippel and C. Quigg, *Phys. Rev. D* **5**, 624 (1972).
- [34] S. Uehara *et al.* (Belle Collaboration), *Phys. Rev. D* **78**, 052004 (2008).
- [35] G. Bonneau *et al.*, *Nucl. Phys.* **54**, 573 (1973).
- [36] T. Feldmann and P. Kroll, *Phys. Lett. B* **413**, 410 (1997).
- [37] S. Uehara (private communication).
- [38] J. Dominick *et al.* (CLEO Collaboration), *Phys. Rev. D* **50**, 4265 (1994).